19th Brazilian Congress of Thermal Sciences and Engineering
November 06th-10th, 2022, Bento Gonçalves - RS - Brazil

ENC-2022-0183
THERMODYNAMIC MODELING OF A HYBRID SOLAR-ELECTRIC DRYER

Gabriel M. B. Cruz
Cristiana Brasil Maia
Pontifícia Universidade Católica de Minas Gerais, Av. Dom José Gaspar, 500, 30535-901 – Belo Horizonte – MG
E-mail: gabriel.cruz@sga.pucminas.br, cristiana@pucminas.br

Abstract. *Drying is a method used worldwide to reduce food losses by increasing its durability. Hybrid dryers can combine the advantages of both natural and artificial dryers by using solar energy as a primary source combined with a supplementary source when needed, such as fossil, biomass, or electric heaters. Therefore, such technique provides a means to minimize the greenhouse effect emission on a commercial scale and mitigate global warming without losing economic feasibility. Hybrid dryers can also guarantee a stable and manageable drying process capable of producing dried food with the quality required in terms of texture, moisture, appearance, taste, and nutritional values. This paper aims at studying a hybrid solar-electric dryer (HSED) without load in Belo Horizonte, MG, Brazil. Based on the first law of thermodynamics, a model was developed to analyze the flow conditions and the feasibility of the HSED. Past research across the world studying solar thermal devices have shown keen interest in energy analyzes as well as successful implementation of solar drying techniques for various agricultural products. The mathematical model developed in this paper proved to be coherent with past studies and can be used to design new dryers and make preliminary analyses.*

Keywords: *thermal modeling, solar drying, hybrid solar-electric drying (HSED), energetic analysis, flow conditions.*

1. INTRODUCTION

According to Mühlbauer & Müller (2020), the most common process for the preservation of agricultural products is drying. When a stored food has too much moisture, there is a high risk for rapid deterioration and spoilage of the product. Open solar drying is an ancient food preservation technique that is still widely used nowadays for being simple, having low investment costs, and not requiring fossil fuels. Some of the downsides of this technique are the food exposure to insects, rodents, and birds; the possibility of contamination with pathogenic; high mass losses due to adverse weather; and de-coloration. In countries with highly mechanized agricultural production, high-capacity and high-temperature automated dryers are applied to dry almost all agricultural products. Fossil fuels are used to heat the drying air, and the fans are driven by electric motors for hot air circulation.

To combine the advantages of both natural and artificial dryers, hybrid dryers are developed by using solar energy as a primary source combined with an auxiliary source when needed, such as fossil, biomass, or electric heaters. According to Martins *et al.* (2008), Brazil has one of the highest levels of insolation in the world. The daily solar irradiation in Brazil varies from 4.25 kWh/m^2 to 6.5 kWh/m^2. Considering that solar energy is an abundant and free energy source, hybrid solar dryers can provide a means to minimize the greenhouse effect emission on a commercial scale and mitigate global warming without losing economic feasibility. Besides that, hybrid dryers can also guarantee a stable and manageable drying process capable of producing dried food with the quality required in terms of texture, moisture, appearance, taste, and nutritional value.

Past researches across the world studying solar thermal devices have shown keen interest in energy and exergy analyses to improve their performance, as well as successful implementation of solar drying techniques for various agricultural products, such as fruits, garlic, carrot, corn, ghost chili pepper, banana, among others. Dhanushkodi *et al.* (2017) studied the drying behavior of cashew in a hybrid solar-biomass dryer (HSBD). They have used fifteen thin layer drying mathematical models to find the best one to describe the collected data of the moisture ratio change for cashew drying. For that, they have analyzed the correlation coefficient (R^2), root mean square error (RMSE), and Reduced Chi-Square. Aghbashlo *et al.* (2009) presented a new mathematical model for the thin-layer drying process. The new model proposed was compared with fifteen previous models and proved to be the best model for the experimental data obtained for the drying of carrots. Rabha *et al.* (2017) used energy and exergy tools to analyze the drying process of ghost chili

pepper and ginger. The results showed an average overall thermal efficiency between 22.95% and 23.30%, an average exergy efficiency of 63% when the ghost chili was dried, and an average exergy efficiency of 47% for the dried ginger. Shreelavaniya *et al.* (2021) developed an indirect active HSBD to study the drying kinetics, mathematical modeling, and quality of dried small cardamom. The dryer could be operated in hybrid (solar and biomass) mode and on biomass only mode to compare the results. The authors used eleven empirical models to find out the most accurate one for their data. The average drying efficiency of the biomass-only mode was 23.98%, and it increased to 28.63% when using the hybrid mode. Although both dryers were within the acceptable limits of microbial quality, the de-coloration was more noticeable in the biomass-only mode. Hadibi *et al.* (2021) analyzed an HSED for garlic drying. They have carried out multiple experiments in different temperatures under natural and forced convection to study the drying kinetics and exergy efficiency. Besides that, they have analyzed the CO_2 mitigation and the payback period of the implementation of the HSED. The exergy efficiency achieved by the dryer used had a range between 69.61% and 89.86%, and the authors concluded that the proposed HSED was found to be sustainable both environmentally and economically. Roratto *et al.* (2021) designed an innovative hybrid solar-electric vacuum dryer to improve the drying time. Vacuum drying can reduce the drying temperature required while increasing the drying rate and producing better sensory and nutritional products when compared with convective drying. Therefore, the authors designed a dryer capable of maintaining the sustainability of solar drying and producing high-quality, homogeneous, and crispy food. Elias *et al.* (2008) studied the nutritional quality and consumer sensory evaluation of dried fuyu persimmons. The authors analyzed moisture content, soluble solids, proteins, lipids, dietary fiber, ascorbic acid, pH, carbohydrates, and minerals before and after the drying process. They have concluded that the drying process was efficient to maintain the nutritional quality of the product while obtaining a high-level acceptance considering the consumer's taste.

The HSED studied in this paper was first developed by Barbosa *et al.* (2018) for an experimental analysis of banana drying. The authors analyzed three methods of drying: the hybrid solar-electric process, the solar process, and the natural sun process. They have succeeded in drying 8 kg of banana slices at a time and concluded that the HSED can combine the advantages of solar and artificial dryers. Besides that, the designed HSED can hegemonically dry the banana slices preventing browning and keeping a satisfactory texture and taste.

In this paper, a mathematical model and an iterative algorithm were developed to analyze the hourly thermal efficiency and the airflow temperature in an HSED without load, based on the model presented for air collectors by Duffie and Beckman (2013). A prototype of the HSED (Fig. 1) was built on the Renewable Energy Studies Group (GREEN), at Pontifical Catholic University of Minas Gerais, Belo Horizonte, MG, Brazil.

Figure 1. Solar Hybrid Dryer.

2. DRYER MODELLING

According to Moran *et al.* (2014), the first law of thermodynamics deals with the quantity of energy and states that energy can neither be created nor destroyed. Therefore, with energy analysis, it is possible to estimate the amount of energy gained from the solar energy in the drying chamber.

From Celma and Cuadros (2009), it was found that the drying process usually depends on the changes produced in the properties of the air. To analyze air's properties during the drying process, it is necessary to determine the values of the main psychrometric variables. Therefore, the ideal gas laws for fluid mixtures are considered, considering that wet air is a one-phase homogeneous system.

As shown in Eq. (1), relative humidity, ϕ, is defined as the ratio between the vapor pressure of water at a given temperature, $p_{v,T}$, and the saturated vapor pressure at the same temperature, $p_{sat,T}$:

$$\phi = \frac{p_{v,T}}{p_{sat,T}}. \tag{1}$$

Specific humidity, ω, can be defined as the mass ratio between the vapor mass, m_w, and the dried air, m_{da}, considering water vapor and drying air as ideal gases. Considering the equation of state of ideal gases, with molar mass 0.2870 g/mol and 0.4615 g/mol respectively, the specific humidity can be defined in Eq. (2):

$$\omega = \frac{m_w}{m_{da}} = \frac{0.2870 \cdot p_{v,T}}{0.4615 p_{a,T}} = 0.622 \frac{p_{v,T}}{P_\infty - p_{v,T}}, \tag{2}$$

in which $p_{a,T}$ is the dried air pressure, and P_∞ is the dead state pressure.

The general equation of mass conservation can be defined as shown in Eq. (3):

$$\dot{m}_{dai} = \dot{m}_{dao} = \dot{m}_{da}, \tag{3}$$

in which $\dot{m}_{dai}$ is the inlet drying air mass flow, $\dot{m}_{dao}$ is the outlet drying air mass flow, and $\dot{m}_{da}$ is the drying air mass flow.

The general equation of mass conservation of moisture can be demonstrated, as shown in Eqs. (4)-(5):

$$\dot{m}_{wi} + \dot{m}_{mp} = \dot{m}_{wo}, \tag{4}$$

$$\dot{m}_{da} \cdot \omega_i + \dot{m}_{mp} = \dot{m}_{da} \cdot \omega_o, \tag{5}$$

in which $\dot{m}_{wi}$ is the inlet water mass, $\dot{m}_{mp}$ is the product/food moisture mass loss, $\dot{m}_{wo}$ is the outlet water mass, ω_i is the inlet specific moisture, and ω_o is the outlet specific moisture.

2.1 Flow conditions

To determine the behavior of the flow inside the solar chamber, an energy balance is performed involving all the heat transfer rates, Fig. 2, based on a similar air heater model proposed by Duffie and Beckman (2013). T is the temperature, Q is the heat transfer, h is the heat transfer coefficient, and the subscript rad is for radiation, $conv$ is for convection, ∞ denotes the ambient conditions, c is for covering, glass in our case, p is for plate, and '-' relates two places (i.e., $h_{conv,c\text{-}p}$ is the convection heat transfer coefficient between the cover and the plate).

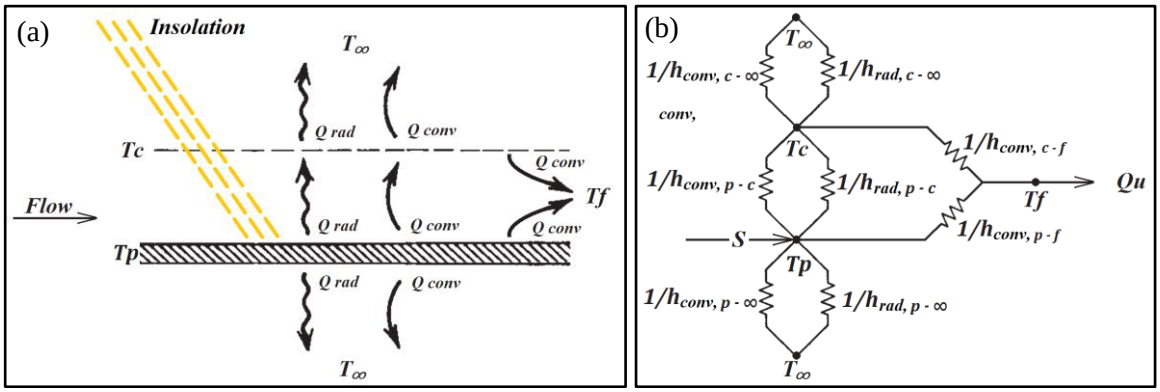

Figure 2. HSED: (a) Energy balance in the collector (b) Thermal network.

According to Duffie and Beckman (2013), the absorbed radiation by the plate, S, can be estimated from Eq. (6), in which, the total incident radiation, I, is given by the sum of three components: a share of direct beam radiation, I_b, a portion of diffuse radiation, I_d, and a portion of radiation reflected by the soil and environment surrounding the dryer, I_g. The term $(\tau\alpha)$ represents the product of transmittance and absorptance values for the direct beam, diffuse, and ground radiation parcels, with the subscripts b, d, and g respectively. The term β represents the angle formed between the collector and a horizontal surface and ρ_g represents the reflectivity of the ground. The geometric factor R_b represents the ratio between the radiation incident on an inclined surface and the radiation incident on a horizontal surface.

$$S = I_b\, R_b (\tau\alpha)_b + I_d (\tau\alpha)_d \left(\frac{1+\cos\beta}{2}\right) + \rho_g\, I (\tau\alpha)_g \left(\frac{1-\cos\beta}{2}\right). \tag{6}$$

It is necessary at first to define the angle of incidence of surfaces, θ_b, the effective ground reflected incidence angle, θ_g, and the effective diffused incidence angle, θ_d.

$$\theta_b = \cos^{-1}[\cos(\phi - \beta)\cos\delta\cos\omega + \sin(\phi - \beta)], \tag{7}$$

$$\theta_g = 90 - 0.5788\,\beta + 0.002693\beta^2, \tag{8}$$

$$\theta_d = 59{,}7 - 0.1388\,\beta + 0.001497\beta^2, \tag{9}$$

in which ϕ is the latitude, δ is the angular position of the sun at solar noon with respect to the plane of the equator, and ω is the hour angle.

The transmittance for each incident radiation component is given by Eq. (10).

$$\tau = \frac{1}{2}\left(\frac{1-r_\parallel}{1+r_\parallel} + \frac{1-r_\perp}{1+r_\perp}\right)\exp\left(-\frac{KL}{\cos\theta_2}\right), \tag{10}$$

in which θ_2 is the angle of refraction, given by Eq. (11), $r_\parallel$ represents the parallel component of unpolarized radiation, given by Eq. (12), $r_\perp$ represents the perpendicular component of unpolarized radiation, given by Eq. (13), K the extinction coefficient, and L is the plate and cover spacing.

$$\theta_2 = \sin^{-1}(n \cdot \sin\theta), \tag{11}$$

$$r_\parallel = \frac{\tan^2(\theta_2 - \theta_1)}{\tan^2(\theta_2 + \theta_1)}, \tag{12}$$

$$r_\perp = \frac{\sin^2(\theta_2 - \theta_1)}{\sin^2(\theta_2 + \theta_1)}, \tag{13}$$

in which n is the average refractive index in the solar spectrum.

The solar absorptance is given by Eq. (14).

$$\alpha = \alpha_n(1 - 1.5879\cdot10^{-3}\theta + 2.7314\cdot10^{-4}\theta^2 - 2.3026\cdot10^{-5}\theta^3 + 9.0244\cdot10^{-7}\theta^4 - 1.8\cdot10^{-8}\theta^5 + 1.7734\cdot10^{-10}\theta^6 - 6.9937\cdot10^{-13}\theta^7), \tag{14}$$

in which α_n is the solar absorptance at normal incidence.

Now, it is possible to calculate $(\tau\alpha)$ for each incident radiation component.

$$(\tau\alpha) = \frac{\tau\alpha}{1-(1-\alpha)\rho_d}, \tag{15}$$

in which ρ_d is the reflectance of the cover system for diffuse radiation incident on the bottom side.

The heat transfer coefficient by radiation between the cover and the ambient, $h_{rad,c\text{-}\infty}$, can be calculated as shown in Eq. (16).

$$h_{rad,c\text{-}\infty} = \varepsilon_c\,\sigma(T_c + T_\infty)(T_c^2 + T_\infty^2), \tag{16}$$

in which ε_c is the glass cover emittance and σ is the Stefan-Boltzmann constant.

Similarly, the heat transfer coefficient by radiation between the plate and the ambient, $h_{rad,p\text{-}\infty}$, can be calculated.

Both convection heat transfer coefficient between the cover and the ambient, $h_{conv,c\text{-}\infty}$, and between the plate and the ambient, $h_{conv,p\text{-}\infty}$, is equal to the wind heat transfer coefficient.

The overall heat transfer coefficient between the cover and the ambient, $U_{c\text{-}\infty}$, and between the plate and the ambient, $U_{p\text{-}\infty}$, is given by Eqs. (17)-(18) respectively.

$$U_{c\text{-}\infty} = h_{rad,c\text{-}\infty} + h_{conv,c\text{-}\infty}, \tag{17}$$

$$U_{p\text{-}\infty} = h_{rad,p\text{-}\infty} + h_{conv,p\text{-}\infty}. \tag{18}$$

The heat transfer coefficient by radiation between the cover and the plate, $h_{rad,p\text{-}c}$, can be calculated by Eq. (19)

$$h_{rad,p\text{-}c} = \frac{\sigma(T_p + T_c)(T_p^2 + T_c^2)}{\frac{1}{\varepsilon_p} + \frac{1}{\varepsilon_c} - 1}, \tag{19}$$

in which ε_p is the plate emittance.

The convection heat transfer coefficient between the cover and the plate, $h_{conv,p\text{-}c}$, can be calculated by Eq. (20).

$$h_{conv,p\text{-}c} = \frac{Nu \cdot k}{L}, \tag{20}$$

in which k is the air thermal conductivity, and Nu is the Nusselt number, given by Eq. (21).

$$Nu = 1 + 1.44\left[1 - \frac{1708(sen\ 1.8\beta)^{1,6}}{Ra\cos\beta}\right]\left[1 - \frac{1708}{Ra\cos\beta}\right]^{+} + \left[\left(\frac{Ra\cos\beta}{5830}\right)^{1/3} - 1\right]^{+}, \tag{21}$$

in which the $+$ exponent means that only positive values of the term in square brackets are to be used, otherwise, use zero, and Ra is the Rayleigh number, given by Eq. (22).

$$Ra = \frac{g(T_p - T_c)L^3}{0.5(T_p + T_c)\nu\ \alpha}. \tag{22}$$

The overall heat transfer coefficient between the cover and the plate, $U_{c\text{-}p}$, is calculated as follows.

$$U_{c\text{-}p} = h_{rad,c\text{-}p} + h_{conv,c\text{-}p}. \tag{23}$$

Therefore, the equation for the cover glass temperature is defined as follows.

$$T_c = T_p - \frac{U_t(T_p - T_a)}{h_{conv,p\text{-}c} + h_{rad,p\text{-}c}}. \tag{24}$$

The convection heat transfer coefficient from the cover and the plate to the environment can be calculated by Eq. (25). Since those coefficients are considered equal, the final temperature is given by the mean of the plate and cover temperature.

$$h_{conv,c\text{-}f} = h_{conv,p\text{-}f} = h_f = \frac{0.0158\ Re^{0,8} \cdot k}{2\ L}. \tag{25}$$

At last, the overall loss coefficient, U_L, is calculated as follows.

$$U_L = \frac{(U_{p\text{-}\infty} + U_{c\text{-}\infty})\left(h_f^2 + 2\ h_f\ U_{p\text{-}c}\right) + 2\ U_{c\text{-}\infty}\ U_{p\text{-}\infty}\ h_f}{2\ h_f\ U_{p\text{-}c} + h_f\ U_{c\text{-}\infty} + h_f^2}. \tag{26}$$

The collector efficiency factor, F', is given by Eq. (27)

$$F' = \frac{2\ U_{p\text{-}c}\ h_f + U_{c\text{-}\infty}\ h_f + h_f^2}{(U_{c\text{-}\infty} + U_{p\text{-}c} + h_f)(U_{p\text{-}\infty} + U_{p\text{-}c} + h_f) - U_{p\text{-}c}^2} \quad . \tag{27}$$

The collector flow factor, F'', is given by Eq. (28).

$$F'' = \frac{\dot{m}\ C_P}{A_c\ U_L\ F'}\left[1 - \exp\left(-\frac{A_c\ U_L\ F'}{\dot{m}\ C_P}\right)\right], \tag{28}$$

in which C_P is specific heat and A_c is the inflow area of the dryer.

Knowing all the heat coefficients, it is possible to calculate the air's temperature after being heated by the solar panel. The actual useful energy gain, Q_u, is calculated as follows.

$$Q_u = A_c\ F' F''[S - U_L(T_i - T_\infty)] = \dot{m}\ C_P\left(T_f - T_i\right). \tag{29}$$

in which T_i is the inlet temperature.

Now, it is possible to calculate the mean temperature of the plate, T_{pm}, with Eq. (31). After calculating the temperature of the plate, the iterative process takes place and all the calculation is repeated until this final value converges.

$$T_{pm} = T_f + \frac{Q_u(1 - F' F'')}{A_c\ F'\ F''\ U_L}. \tag{30}$$

2.2 Energy analysis

By the first law of thermodynamics, the general equation of energy conservation can be defined as follows:

$$\sum \dot{E}_i = \sum \dot{E}_o, \tag{31}$$

in which the total energy input, $\dot{E}_i$, is equal to the total energy output, $\dot{E}_o$.

Equation (32) is used to determine the net heat rate, $\dot{Q}$. Note that the change in the potential and kinetic energy were neglected:

$$\dot{Q} = \sum \dot{m}_{ao} h_{ao} - \sum \dot{m}_{ai} h_{ai}, \tag{32}$$

in which h_{ao} is the outlet air specific enthalpy, and h_{ai} is the inlet air specific enthalpy.

The solar heat energy input, $\dot{Q}_u$, was previously defined in Eq. (29).

The energy utilization rate on the electric heater, $\dot{W}_{ele}$, can be defined as the product of the electric tension, V_{ele}, and the electric current, I_{ele}, as shown in Eq. (33).

$$\dot{W}_{ele} = V_{ele} \cdot I_{ele}. \tag{33}$$

The schematics of the drying system can be seen in Fig. 3.

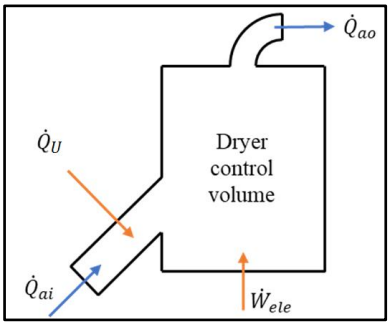

Figure 3. Energy flow diagram of the drying chamber.

The general equation of energy conservation for the dryer can be seen as follows:

$$\dot{Q}_u - \dot{W}_{ele} + \dot{Q}_{ai} - \dot{Q}_{ao} = 0, \tag{34}$$

$$I_S \cdot A_S - V_{ele} \cdot I_{ele} + \dot{m}_{da} \cdot (h_{dai} - h_{dao}) - \dot{m}_{mp} \cdot h_{mp} = 0, \tag{35}$$

in which $\dot{Q}_{ai}$ is the inlet airflow energy, $\dot{Q}_{ao}$ is the outlet airflow energy, h_{dai} is the inlet drying air enthalpy, h_{dao} is the outlet drying air enthalpy, and h_{mp} is the lost moisture enthalpy.

Equation (36) defines the enthalpy of airflow, h_a:

$$h_{ai} = C_{p_a} \cdot T_a + \omega \cdot h_{sat,T}, \tag{36}$$

in which C_{p_a} is specific heat of air and T_a is air temperature.

The thermal efficiency, ηt, of the system can be calculated as follows:

$$\eta t = \frac{\dot{m}_{da} \cdot C_{p_a} \cdot (T_o - T_\infty)}{\dot{Q}_u + V_{ele} \cdot I_{ele}}. \tag{37}$$

3. METHODOLOGY

The HSED used in this paper was developed and is located in the Renewable Energy Studies Group (GREEN), at the Pontifical Catholic University of Minas Gerais, Belo Horizonte, MG, Brazil (latitude 19.9°S and longitude 43.9°W). The dryer is divided into a solar chamber, that is tilted 30º from the horizontal, and a drying chamber, where the products are dried and where the electric heater is located. The drying chamber is 1.74 m long, 1.30 m wide, and 0.435 m deep, with a cover glass 6 mm thick. The walls of the HSED are made with galvanized steel plates painted in matte black.

To estimate the increase of the air's temperature due to insolation and the hourly thermal efficiency, an algorithm was developed. The flowchart in Fig. 4 comprises the steps used. The weather data used was based on a Solar and Wind Energy Resource Assessment (SWERA) standard data of Belo Horizonte (Langle, 2017). Following those steps provides information of the cover, the plate, and the air temperature at any hour of any day at any city. In this study, the iterations stopped when the value was equal to the previous one by two decimal places.

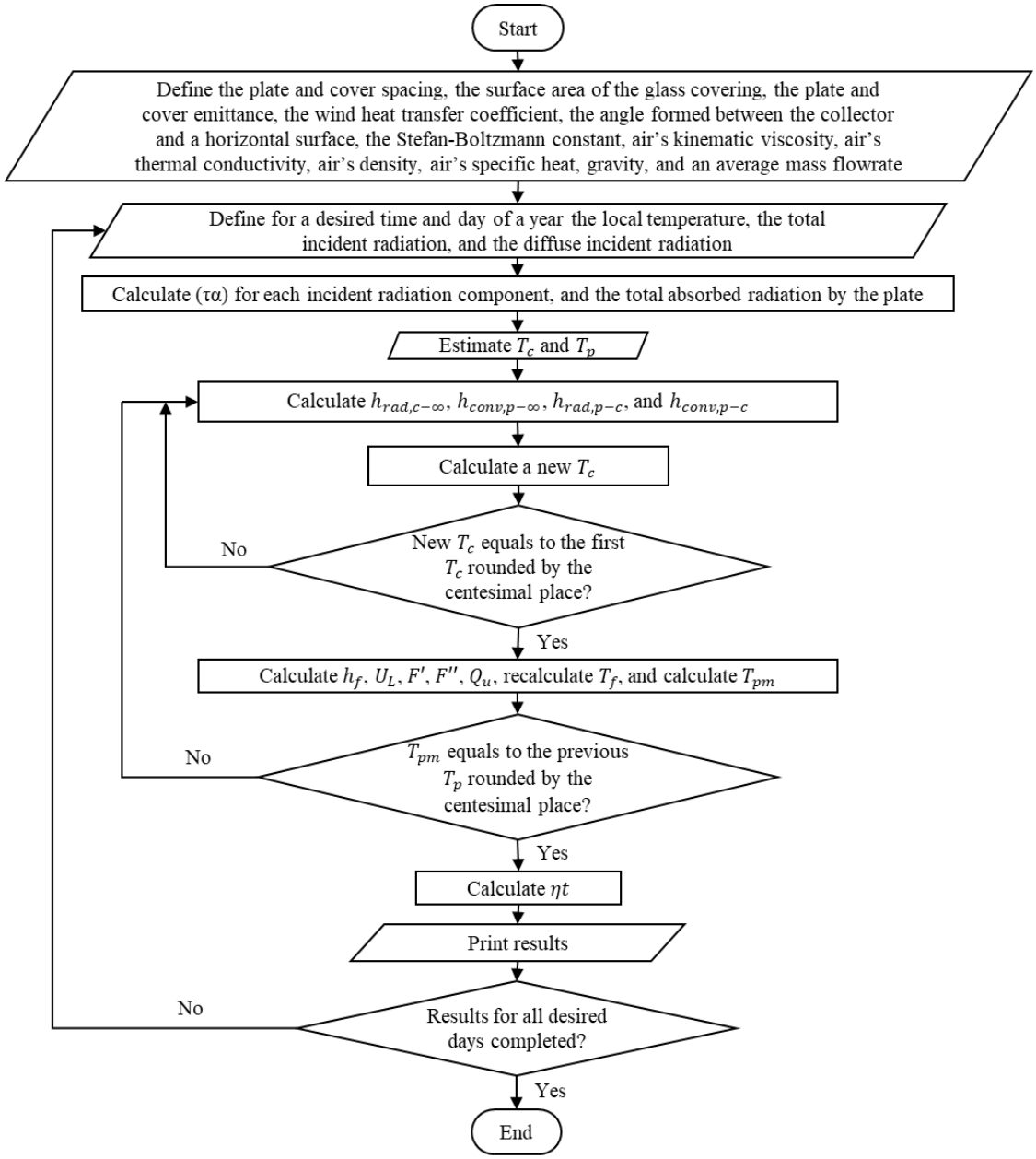

Figure 4. Algorithm flowchart.

4. NUMERICAL RESULTS

A thermodynamic analysis based on the first law of thermodynamics was performed for four days of the year: autumn equinox (March 31st), winter solstice (June 21st), spring equinox (September 22nd), and summer solstice (December 21st) in the southern hemisphere. These particular days were selected because they represent the beginning of each season. Besides that, those dates have different insolation characteristics, temperatures, and solar paths. The analyses were taken between hours 6 and 18 because this time range covers most of the day insolation throughout the year. The reference location for this study was Belo Horizonte.

Figure 5 shows, for the four different days, the hourly numerical results of ambient temperature (Ta), airflow temperature at the inlet of the drying chamber (Tf), and the plate surface temperature (Tp). Solar irradiance is also shown to help the evaluation of the results.

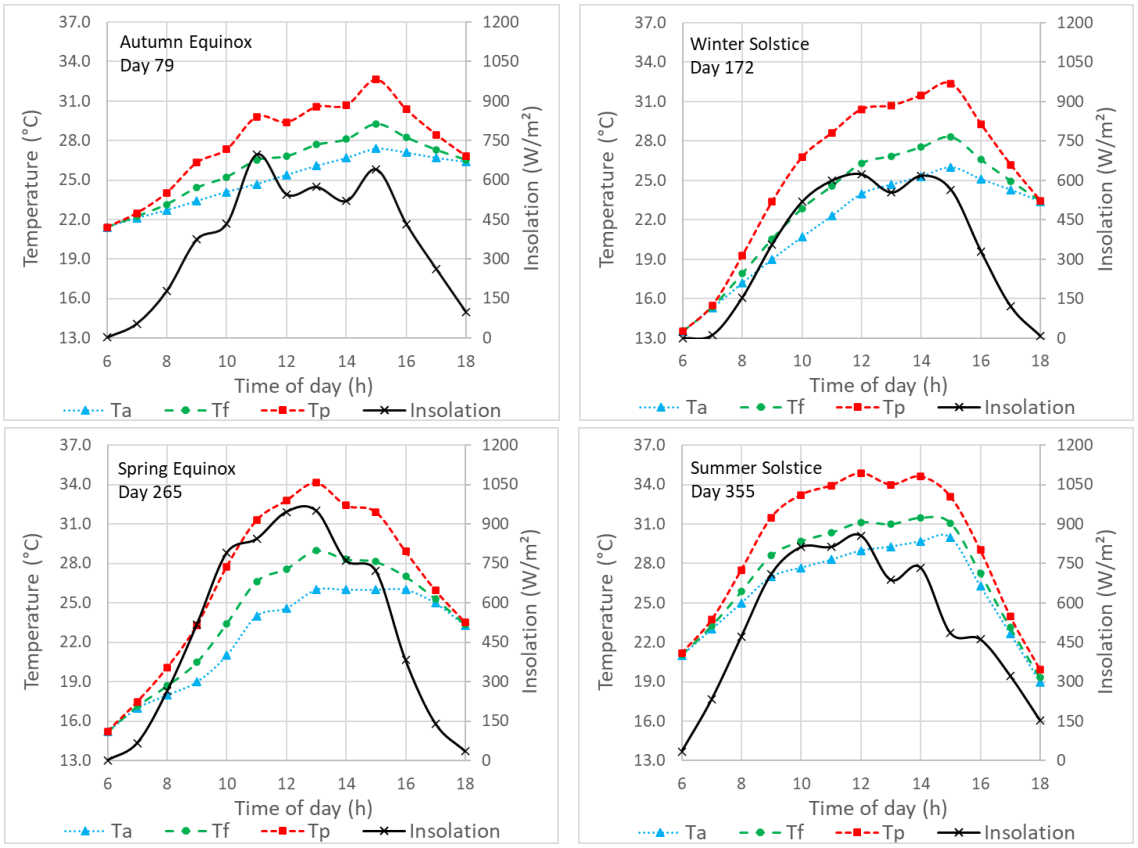

Figure 5. Hourly insolation, ambient temperature data (Ta), and the numerical results airflow temperature after solar heating (Tf) and plate temperature (Tp) during autumn equinox, winter solstice, spring equinox, and summer solstice in the HSED at Belo Horizonte.

It can be seen that the solar irradiance is higher in spring and summer, and lower in autumn and winter. The ambient temperature is higher in the summer solstice. During the day, the behavior of the airflow and plate surface temperatures is the same of the solar irradiance, increasing in the morning and decreasing in the afternoon. For a given time, as expected, the plate temperature is higher than the ambient temperature. Besides that, the heated airflow temperature is a value in between the plates and the ambient temperature.

Figure 6 shows the hourly thermal efficiency for the autumn equinox, winter solstice, spring equinox, and summer solstice. The behavior of the thermal efficiency follows the behavior of the solar irradiance and temperatures, increasing in the morning and decreasing in the afternoon. It can be seen that the values were close.

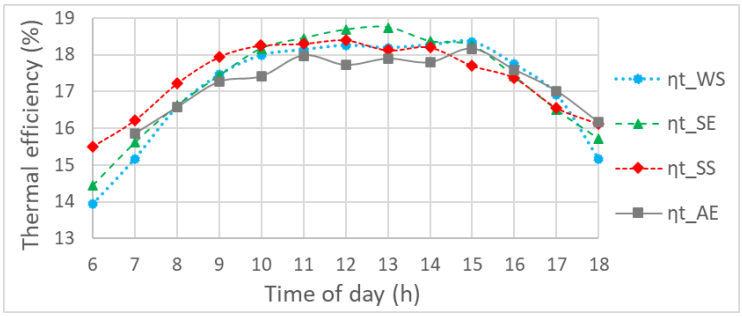

Figure 6. Hourly thermal efficiency (ηt) for the autumn equinox (AE), winter solstice (WS), spring equinox (SE), and summer solstice (SS).

Comparing the thermal efficiency with the data of previous studies carried out on the same HSED (Senna *et al.*, 2019), the numerical results seen in Fig. 6 were within the expected order of magnitude and proportion. The difference in results is attributed to variations in environmental parameters. The inlet air temperature, for instance, plays an important role in the efficiency. To assess this influence, the inlet air temperature was varied from 1 to 4 °C higher than the ambient temperature, and the average thermal efficiency on autumn equinox varied from 9.06 to 43.65%.

Table 1 shows the average values of temperatures (Ta, Tp, and Tf), insolation, thermal efficiency (ηt), and relative temperature increase of each desired day, with the standard error of the mean (SEM), defined as the ratio between the sample standard deviation and the root of its size, with a confidence level of 68.27% (Montgomery and Runger, 2021).

Table 1. Average temperatures, insolation, and thermal efficiency with the respective SEM.

	Ta (°C)	Insolation (W/m²)	Tp (°C)	Tf (°C)	$(Tf - Ta)/Ta$ (%)	ηt (%)
Autumn equinox	24.9 ± 0.6	370 ± 64 (±17%)	27.7 ± 0.9	25.9 ± 0.7	4.0	16.0 ± 1.3
Winter solstice	21.6 ± 1.1	343 ± 70 (±20%)	25.4 ± 1.7	23.0 ± 1.3	6.5	17.1 ± 0.4
Spring equinox	22.4 ± 1.1	494 ± 100 (±20%)	26.5 ± 1.7	23.9 ± 1.3	6.7	17.3 ± 0.4
Summer solstice	26.0 ± 1.0	522 ± 76 (±15%)	29.3 ± 1.5	27.2 ± 1.2	4.6	17.4 ± 0.3

As shown in Tab. 1, the SEM uncertainties serve to show whether or not the mean values differ significantly from each other. For example, Ta of autumn (varying from 24.3 to 25.5 °C) and Tp of autumn (varying from 26.8 to 28.6 °C), do not intersect. The increase in the relative temperature shows that the gained heat in the summer and autumn was slightly lower because the ambient temperature was already higher. On the other hand, the relative temperature increase was greater in the winter and spring, when the ambient temperature was lower, with lower insolation. Moreover, it is noticeable that the summer solstice in Belo Horizonte has the highest temperatures and insolation with the lowest insolation percentual SEM, ensuring the best thermal efficiency. However, the thermal efficiencies of each day have relatively close values. Compared with countries in North America or in Europe, it is possible to notice on the data the tropical weather characteristics, such as a relatively stable temperature throughout the year, with stable temperatures and insolation.

As an example of how the developed model can be applied for different analyses, Fig. 7 shows the impact of the wind heat transfer coefficient value on the final temperature and the thermal efficiency. It is important to highlight that the convective heat transfer depends on wind speed. A dryer in a windier location will have greater convective heat losses, and lower airflow outlet temperatures.

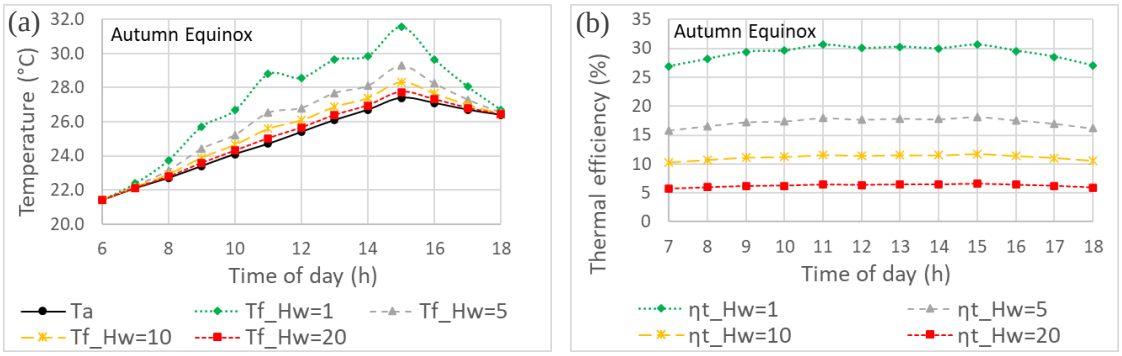

Figure 7. (a) Ambient and final temperatures and (b) thermal efficiency for different values of wind heat transfer coefficient (Hw = 1, 5, 10, and 20 W/m²K) for the autumn equinox.

By the analysis presented in Fig. 7, the wind heat transfer coefficient has a considerable impact on the final temperature and the dryer's thermal efficiency. Therefore, it is preferable to install the dryer in a less windy location.

5. CONCLUSIONS

This paper presented a mathematical model and an iterative algorithm developed to analyze the thermal efficiency and the airflow temperatures on an HSED without load built on GREEN, located in Belo Horizonte, MG, Brazil. To analyze the dryer in different ambient conditions, both equinoxes and solstices were chosen to be the studied days. The data used for the numerical analysis was accordingly to the dryer location for each desired hour and day.

The algorithm results proved to be within the expected order of magnitude and proportion, and the iterative computation converged as expected. The airflow temperature after solar heating was higher than the ambient temperature and lower than the temperature of the plate. Besides that, it was noticeable the correlation of the hourly insolation with the calculated temperatures. The numerical results also proved that the designed dryer has a stable thermal efficiency along different seasons of the year and that the hourly thermal efficiency increases around noon and decreases in the afternoon.

The presented methodology can be used for dryer modeling with moderate ease and flexibility. It is possible to adapt the model for different dryer designs, such as adding insulation on the back of the dryer or adding any number of glass covers. And it can be used to tweak certain parameters of the dryer, such as the distance between the plate and the glass cover, the material used for each part of the dryer, and the dryer geometry, among others. With that, it is possible to make

a preliminary analysis of the dryer before its construction. For example, it was noticed that the wind conditions have a considerable influence on the final result.

Therefore, the current study presented an analysis tool development that achieved results in agreement with previous studies, which concluded that the present HSED is suitable as an alternative dryer for bananas while using a renewable energy source as a primary source and complementing it with an electric source when needed.

6. ACKNOWLEDGEMENTS

This study was financed in part by the Coordenação de Aperfeiçoamento de Pessoal de Nível Superior - Brasil (CAPES) – Finance Code 001. The authors are also thankful to PUC Minas, FAPEMIG, and CNPq.

In memoriam of my grandfather, who always encouraged my studies.

7. REFERENCES

Aghbashlo, M., Kianmehr, M.H., Khani, S. and Ghasemi, M., 2009. Mathematical modelling of thin-layer drying of carrot. *International Agrophysics*, Vol. 23, No. 4, pp. 313-317.

Barbosa, E.M.C., Maia, C.B., Zidan, D.C., Barbosa, R.R.C., Santana V.A.C. and Diniz A.S.A.C., 2018. "Experimental Analysis of Banana Drying in an Electric Hybrid Solar Dryer". In *Brazilian Congress of Thermal Engineering and Sciences – ENCIT 2018*. Águas de Lindóia, Brazil.

Celma, A.R. and Cuadros, F., 2009. Energy and exergy analyses of OMW solar drying process. *Renewable Energy*, Vol. 34, No. 3, pp. 660-666.

Dhanushkodi, S., Wilson, V.H. and Sudhakar, K., 2017. Mathematical modeling of drying behavior of cashew in a solar biomass hybrid dryer. *Resource-Efficient Technologies*, Vol. 3, No. 4, pp. 359-364.

Duffie J.A. and Beckman W.A., 2013. *Solar Engineering of Thermal Processes*. John Wiley & Sons, Inc., Hoboken, Unites States of America, 4th edition.

Elias, N.F., Berbert, P.A., Molina, M.A.B., Viana, A.P., Dionello, R.A. and Queiroz, V.A.V., 2022. Avaliação nutricional e sensorial de caqui cv Fuyu submetido à desidratação osmótica e secagem por convecção. *Ciência e Tecnologia de Alimentos*, Vol. 28, No. 2, pp. 322-328

Hadibi, T., Boubekri, A., Mennouche, D., Benhamza, A. and Abdenouri, N., 2021. 3E analysis and mathematical modelling of garlic drying process in a hybrid solar-electric dryer. *Renewable Energy*, Vol. 170, pp. 1052-1069.

Langle, N., 2017. "SWERA" OpenEI. 6 Jul. 2022 < https://data.openei.org/submissions/425 >

Martins, F.R., Pereira, E.B., Abreu, S.L.d. and Colle, S., 2008. "Brazilian Atlas for Solar Energy Resource: Swera Results". In *Proceedings of ISES World Congress 2007: Solar Energy and Human Settlement*. Heidelberg, Germany.

Montgomery, D.C. and Runger, G.C., 2021. *Estatística Aplicada e Probabilidade para Engenheiros*. LTC, Rio de Janeiro, Brazil, 7th edition.

Moran, M.J., Shapiro, H.N., Boettner, D.D. and Bailey, M.B., 2014. *Fundamentals of Engineering Thermodynamics*. John Wiley & Sons, Inc.,. Kendallville, Unitted Stats of America, 8th edition.

Mühlbauer, W. and Müller, J., 2020. *Drying Atlas: Drying Kinetics and Quality of Agricultural Products*. Woodhead Publishing, an imprint of Elsevier, Duxford, 1st edition.

Rabha, D.K., Muthukumar, P. and Somayaji, C., 2017. Energy and exergy analyses of the solar drying processes of ghost chilli pepper and ginger. *Renewable Energy*, Vol. 105, pp. 764-773.

Roratto, T.B., Monteiro R.L., Carciofi, B.A.M. and Laurindo, J.B., 2021. An innovative hybrid-solar-vacuum dryer to produce high-quality dried fruits and vegetables. *LWT*, Vol. 140, No. 110777.

Senna, C.M., de Castro, G.W.M., de Souza, L.R.M., 2019. *Análise energética e exergética do processo de secagem de banana em um secador híbrido solar elétrico*. Monography thesis, Pontificial Catholic University of Minas Gerais, Belo Horizonte, Brazil.

Shreelavaniya, R., Kamaraj, S., Subramanian, S., Pangayarselvi, R., Murali, S. and Bharani, A., 2021. Experimental investigations on drying kinetics, modeling, and quality analysis of small cardamom (Elettaria cardamomum) dried in solar-biomass hybrid dryer. *Solar Energy*, Vol. 227, No. 11, pp. 635-644.

8. RESPONSIBILITY NOTICE

The authors are the only responsible for the printed material included in this paper.